Recyclable holographic interferometer with a photorefractive crystal: optical scheme optimization

S. V. Miridonov

Centro de Investigación Científica y Educación Superior de Ensenada, A.P. 2732, 22800 Ensenada, México

A. A. Kamshilin

University of Joensuu, P.O. Box 111, SF-80101 Joensuu, Finland

E. Barbosa

Universidade Estadual de Campinas, Cx. P. 6165, 13081 Campinas, SP, Brazil

Received November 11, 1992; revised manuscript received October 13, 1993; accepted January 10, 1994

Holographic image formation in photorefractive crystals with use of a complex object wave front is studied both theoretically and experimentally. It is shown that the optimal conditions for holographic recording of a complex image differ from those required when a plane wave front is used as an object beam. Experimental measurements of the hologram's diffraction efficiency and the optical noise dependencies on the recording-beam polarization and intensity ratio are in good agreement with theory. An experimental approach designed to find the optimal configuration of optical elements in a holographic interferometer with a photorefractive crystal is presented.

1. INTRODUCTION

Photorefractive crystals (PRC's) are useful as hologram recording media in holographic interferometry because of their practically unlimited recyclability and sufficiently high sensitivity. No chemical or physical processing is needed for visualizing optical information recorded in these crystals; therefore the image (holographic interferogram) reconstructed from the hologram can be observed simultaneously with the hologram recording. Different optical schemes that realize the simultaneous holographic recording and reconstruction in PRC's have been proposed for designing holographic interferometers, such as wave-front conjugation (four-wave mixing),[1] two-wave holographic amplification,[2] and anisotropic self-diffraction.[3]

One serious problem with any holographic interferometer is the quality of the reconstructed interferograms (images), which can be strongly restricted by light scattered in the image direction (optical noise). Only a limited number of studies that deal with the optical noise problem for holograms recorded in PRC's have appeared in the literature.[4–6] Usually the experimental data are obtained when both the reference and the object waves have plane (or near-plane) wave fronts. But it is more important from a practical point of view to study holographic image formation in the case in which the object beam has a complex wave front formed by light diffusely scattered from the object.

This paper presents for the first time, to our knowledge, theoretical and experimental studies of holographic image formation for a complex object wave. The results have allowed us to optimize the optical scheme of a recyclable (dynamic) holographic interferometer on the basis of the use of PRC's. Among the different types of PRC that are available now, the crystals of the sillenite family ($Bi_{12}SiO_{20}$, $Bi_{12}TiO_{20}$, and $Bi_{12}GeO_{20}$) possess a higher sensitivity that enables them to record holograms in the visual region of the spectrum. It is not so difficult to grow sillenite-type single crystals of large size and high optical quality, which is very important for holographic recording of complex images. Moreover, $Bi_{12}TiO_{20}$ (BTO) crystals are sensitive to red light,[7] so that it is possible to use a widely spread He–Ne laser as a source of coherent light.

2. DUAL-BEAM HOLOGRAPHIC INTERFEROMETER

There are a variety of optical schemes that permit the reconstruction of complex images from volume holograms in PRC's. The common feature of all of them is that from every beam illuminating the crystal at the moment of the reconstruction some light is scattered in the direction of the reconstructed image. This scattered light is optical noise for the image that is reconstructed from the hologram. The two principal sources of noise are the object beam and the reconstructing beam. For our experimental study we chose a dual-beam scheme of simultaneous hologram recording and reconstruction[3] because of its simplicity and high fidelity. In this scheme the reference beam serves simultaneously as a reconstructing beam, and Bragg's conditions of diffraction from volume holograms are automatically fulfilled. Even though the experimental data were obtained for a particular optical scheme, they can also be applied to the optimization of other kinds of holographic interferometers with PRC's.

The configuration of the dual-beam holographic interferometer is shown in Fig. 1. The light scattered (or

0740-3232/94/061780-09$06.00

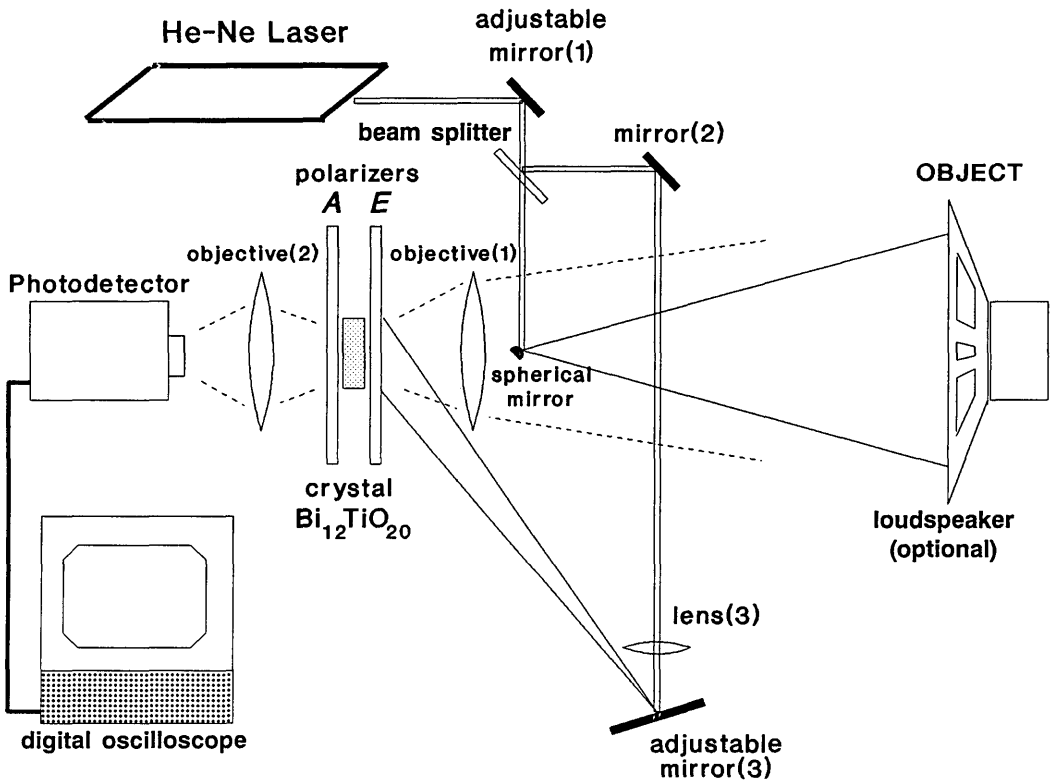

Fig. 1. Scheme of the dual-beam holographic interferometer.

refracted) by the object being tested is focused by objective (1) into the volume of the sample. The reference beam crosses the object beam inside the sample under angle ϑ (see Fig. 2 below), which determines the average (carrier) spatial frequency f of the recorded hologram. It is well known[8] that holograms recorded in PRC's of the sillenite family are more effective when the optical faces of the sample are parallel to the crystallographic surface [110]. The diffraction from these holograms has an anisotropic character resulting from the symmetry of the PRC, reflected in the tensor form of its electro-optic coefficients. Because of this anisotropy, light diffracted by PRC holograms can be accompanied by rotation of the plane of polarization[9] for a chosen crystal orientation. Therefore the beam diffracted from the hologram (the reconstructed complex image) can be separated from the transmitted beam by the placement of a properly oriented analyzer behind the crystal.[3] So the reconstructed image, as well as the holographic interferogram, can be observed continuously and simultaneously with the recording process.

The objective of any holographic interferometer is to obtain information about displacements and vibrations of the object through measurements of object-beam wavefront differences. This information is contained in the diffracted wave, and hence the intensity of that wave may be regarded as the signal power. All other light collected by the objective (2) in Fig. 1 is noise. There are only two noise sources for the dual-beam holographic interferometer of Fig. 1: the transmitted object beam, with noise power P_{NO}, and the scattered reference beam, with noise power P_{NR}. We suppose that both P_{NO} and P_{NR} are proportional to the intensity of the object beam and of the reference beam, respectively. This assumption is in rather good accordance with the experimental results that we obtained by using a 10-mW He–Ne laser in our experiments.

For some applications, such as holographic memory and interconnections, the hologram in a PRC can be reconstructed by use of only one reconstructing (reference) beam. In this case the object-beam noise P_{NO} is absent, and only P_{NR} should be estimated. But for real-time interferometers based on photorefractive crystals, it seems to be more convenient to use simultaneous recording and reconstruction, because it allows one to obtain stationary values of diffraction efficiency. In this case the quality of the reconstructed image will be limited by both P_{NO} and P_{NR}. In the present paper we analyze the latter case in more detail, because we consider it more interesting and more important for holographic interferometry.

3. THEORETICAL ANALYSIS

The main goal of the theoretical analysis is to estimate the signal-to-noise ratio (SNR) in the image of a diffusely scattering light object that is reconstructed from a hologram recorded in a photorefractive crystal. This study considers a hologram of a focused image in the case in which the reference beam has a plane wave front. We use the common definition of SNR as the ratio between the average output signal power, which is determined here as the average light intensity of the reconstructed object wave, and the average noise power, which is the total average intensity of undesirable background in the plane of the reconstructed image. The undesirable background, or optical noise, is assumed to be produced by light scattered from the reference beam and by the object beam and transmitted to the reconstructed image

plane. In this paper we take into account only the final influence of the scattered optical noise on the reconstructed image quality. We do not consider how the noise arises inside the crystal. The origin of the noise might be either scattering on both crystal volume imperfections and input–output surface defects or Rayleigh scattering (for extremely high-quality crystals) or all these reasons together. Our main assumption is that there is direct proportionality of scattered noise power P_{NR} to the light intensity of the reference beam I_{RE} (the proportionality was checked experimentally). The transmitted part (but not the reconstructed part) of the object beam also produces undesirable background in the reconstructed image and, as a result, decreases the contrast of time-average or double-exposure interferograms. The power of this noise component P_{NO} is proportional to the average intensity of the object beam, $\langle I_{OB}\rangle = \langle |B(x,y)|^2\rangle$, where $B(x,y)$ is the complex amplitude distribution of the object wave in the image plane. Hence the noise power is assumed to be the sum of two components, $P_{NR} = n_R I_{RE}$ and $P_{NO} = n_O\langle I_{OB}\rangle$, where n_R and n_O are the proportionality coefficients for the reference and the object beams, respectively.

The average intensity of the reconstructed wave is

$$\langle I_S\rangle = \langle |S(x,y)|^2\rangle , \tag{1}$$

where $S(x,y)$ is the two-dimensional complex amplitude distribution of the reconstructed wave in the image plane. Hence, in accordance with the definition given above,

$$\mathrm{SNR} = \frac{\langle |S(x,y)|^2\rangle}{n_R I_{RE} + n_O\langle I_{OB}\rangle} . \tag{2}$$

In order to define the average intensity of the reconstructed wave, we should take into account some features of hologram recording when the object wave comes from a diffusely scattering light object. Such objects produce complex object waves with a wide spectrum of spatial frequencies. The light intensity in these waves is distributed in space in accordance with an exponential probability law,[10] and the pattern formed by such waves is usually known as speckle. In coherent imaging this speckle is sometimes recognized as noise. However, this complex object wave is the input signal that is used for recording the hologram in a photorefractive crystal, and it has to be reconstructed with a high SNR. Therefore in our analysis we consider the entire object wave not as noise but as a complex wide-band signal. Because of this noiselike structure of the object wave, we use the known statistical properties, the average light intensity, and the probability-density function associated with the light intensity of speckle patterns to describe this input signal in order to determine the average intensity of the reconstructed wave. In other words, the object wave front is considered here to be a sample function of a two-dimensional random process.[10]

The reconstructed wave amplitude naturally depends on the hologram diffraction efficiency η, and we used the saturation value for η in the SNR calculation because that is maximum value. The diffraction efficiency of a volume hologram in an optically active PRC of the sillenite type depends on the electric-field amplitude $\mathbf{E}_{SC}$ of redistributed space charges inside the crystal,[3] and for small η (considering that both recording beams are plane wave fronts) it can be expressed in the form

$$\eta = \left(\frac{\pi n^3 r_{41}\mathbf{E}_{SC}}{2\lambda\cos\vartheta} \frac{\sin(\rho\mathbf{d})}{\rho} \right)^2 , \tag{3}$$

where n is the refractive index of the crystal, r_{41} is the electro-optic coefficient, λ is wavelength of the recording light, ϑ is the angle between recording beams, ρ is the optical rotatory power (in radians per millimeter), and $\mathbf{d}$ is the crystal thickness (assuming that the hologram occupies all the space between the input and the output crystal faces). It is necessary to note that the small-diffraction-efficiency assumption allows us to neglect the influence of the interference between recorded and diffracted beams on additional hologram recording and erasure. In other words, the energy-exchange effect is neglected in our theoretical treatment.[11]

The saturated $\mathbf{E}_{SC}$ is independent of the total intensity of the recording beams,[8] but it is proportional to the interference-pattern modulation index m, i.e., to the reference- to-object-beam-intensity ratio. When both object and reference waves are plane, the complex object-beam amplitude B and its intensity $I_{OB} = |B|^2$ are constants:

$$\mathbf{E}_{SC} \sim m = \frac{2(I_{RE}I_{OB})^{1/2}}{I_{RE} + I_{OB}} = \frac{2|A^*B|}{|A|^2 + |B|^2} , \tag{4}$$

where A is the complex amplitude of the reference beam ($I_{RE} = |A|^2$). The complex amplitude of the reconstructed wave, S, in this case is proportional to

$$S \sim \frac{A^*BC}{|A|^2 + |B|^2} , \tag{5}$$

where C is the amplitude of the readout wave. Hence the intensity of the reconstructed beam

$$I_S \sim \frac{I_{RE}I_{OB}I_C}{(I_{RE} + I_{OB})^2} , \tag{6}$$

where $I_C = |C|^2$ is the intensity of the readout beam. When self-diffraction is used (the reference beam is also the readout beam at the same time: $I_C = I_A$), the reconstructed wave intensity is

$$I_S(I_{RE}, I_{OB}) \sim \frac{{I_{RE}}^2 I_{OB}}{(I_{RE} + I_{OB})^2} . \tag{7}$$

Substituting relation (7) into Eq. (2), we obtain the SNR for recording beams with plane wave fronts:

$$\mathrm{SNR}_{pl} \sim \frac{{I_{RE}}^2 I_{OB}}{(I_{RE} + I_{OB})^2(n_R I_{RE} + n_O I_{OB})} . \tag{8}$$

But in our case, because of the diffusely scattered light coming from the object, the value $I_{OB} = |B|^2$ in relations (4)–(7) is a function of the coordinates as a result of the nonuniformity of the object wave, which has a speckle-type intensity distribution. However, the local value I_S at some point (x,y) can be written by relation (7) if the local value of I_{OB} at the same point is substituted. Therefore one can calculate the average intensity of the reconstructed beam $\langle I_S\rangle$ [Eq. (1)] by averaging I_S in

relation (7), taking into account the statistical properties of the object wave.

It is known[10] that the light intensity of a speckle pattern is distributed by the exponential probability law:

$$p(I_{OB}) = \frac{\exp(-I_{OB}/\langle I_{OB}\rangle)}{\langle I_{OB}\rangle}. \tag{9}$$

The average value of the intensity of the reconstructed beam can be calculated now by use of relations (7) and (9):

$$\langle I_S\rangle = \int_0^\infty I_S(I_{RE}, I_{OB}) p(I_{OB}) \mathrm{d}I_{OB} \sim I_A a \int_0^\infty \frac{x \exp(-x)}{(a+x)^2} \mathrm{d}x. \tag{10}$$

Here parameter a describes the reference-to-object-beam intensity ratio: $a = I_{RE}/\langle I_{OB}\rangle$. By substituting relation (10) into Eq. (2) one can get the final expression for the SNR:

$$\mathrm{SNR} \sim \frac{a^2}{n_R a + n_O} \int_0^\infty \frac{x \exp(-x)}{(a+x)^2} \mathrm{d}x. \tag{11}$$

Analysis of this expression shows that the dependence of the SNR on the reference-to-object-beam intensity ratio has a maximum whose position depends on both coefficients n_R and n_O. Hence the optimization of the holographic interferometer with PRC's in the self-diffraction mode requires that one take into account both noise components. But the case of $n_O = 0$ also has special importance, because it represents the typical situation in which the recorded hologram is illuminated only by the readout beam, as it is in holographic memory systems, for example. In this case the SNR for a hologram of a complex object wave attains its maximum value when $a \approx 0.7$, as follows from relation (11). This means that the optimal conditions for the holographic recording of a complex object correspond to a reference-beam intensity that is 30% less than the object-beam intensity. This result differs from the one obtained for the case of a holographic recording of an object wave whose intensity distribution is more-or-less uniform over the crystal volume. One can see from relation (8) that for the hologram reconstruction case ($n_O = 0$) that maximal SNR is achieved when both recording beams have equal intensity $a = 1$; this is a well-known fact. Experimental data presented here for complex object wave hologram recording are in good agreement with the theoretical calculations shown above.

4. EXPERIMENTAL PROCEDURE

Experimental measurements of holographic parameters for a BTO crystal were carried out in the holographic interferometer whose configuration is shown in Fig. 1. The laser beam generated by the 10-mW He–Ne laser is divided into two beams: the object beam and the reference beam. Then the object beam is reflected by a spherical micromirror, where it expands and illuminates the object. The light backscattered from the object surface is collected by an objective (1) into the crystal volume. Such a configuration of the object arm allows measurement of displacements (or vibrations) of the object surface in the direction of the illuminated beam without the need for any geometrical factor correction ($\cos 2\beta$). Furthermore, in this configuration retroreflective paint can be used quite effectively. The spherical micromirror is locked near objective (1) and does not significantly influence the quality of the image.

The reference beam is reflected by a firmly fixed mirror (2), passes through lens (3), and then is reflected by an adjustable mirror (3) to reach the crystal surface. The reference-beam path is more or less equal to the object-beam path. The size of the light spot from the reference beam on the crystal surface is expanded by lens (3) to provide a complete cross section of the reference and the object beams into the crystal volume.

The reference beam and the object beams interfere in the crystal volume to record a dynamic hologram, which is simultaneously reconstructed by use of the same reference beam. Two BTO samples of sizes $7.5 \times 8.0 \times 8.8$ mm^3 (BTO48) and $6.1 \times 7.5 \times 8.0$ mm^3 (BTO53) were used in our experiments. Both single crystals were grown in the Department of Quantum Electronics of the A. F. Ioffe Physical-Technical Institute (St. Petersburg, Russia). The PRC orientation used in this work is shown in Fig. 2. The hologram vector is perpendicular to the [001] axis of the crystal. The sample holder was made from insulated plastic and can hold two polarizers very close to the crystal surfaces. Polarizer sheets can be rotated manually for adjustment of the system, but they are firmly fixed during the interferometer work.

A fixed surface covered by retroreflective paint was used as a test object to measure the holographic parameters of the crystal. The illuminated spot diameter on the object surface is approximately 15 mm. The image diameter focused into the crystal is approximately 2 mm. Note that all our measurements were carried out for the complex object beam wave front, whose spatial bandwidth in the crystal is near 400 cycles/mm. The object beam, transmitted through the two polarizers and the crystal between them, is focused by lens (3) (see Fig. 1) onto a photodetector with a sensitive area 10% larger than the measured image area. The photodetector was connected to a digital oscilloscope for recording of photocurrent evolution. Over the whole set of measurements the light in-

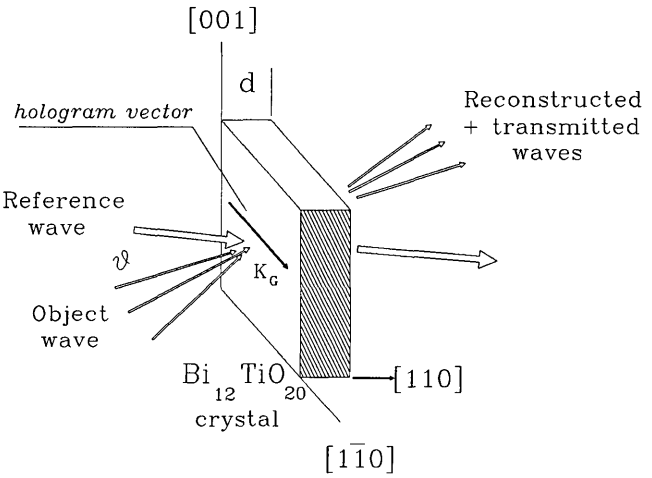

Fig. 2. Orientation of the photorefractive crystal $Bi_{12}TiO_{20}$ in the holographic interferometer. ϑ, Bragg angle.

tensity in the photodetector was much smaller than the saturation value.

There are three main parameters of the optical scheme of a self-diffraction holographic interferometer, which can be varied to produce a high-quality holographic interferogram. The first is the polarization angle of the recording beams, which is determined by the orientation of the polarizer E (see Fig. 1). The second is the reference-to-object-beam intensity ratio, which depends on the beam-splitter rate and on the areas of the beams at the crystal plane. The third is the spatial frequency of the hologram that is being defined by the angle between recording beams. The first and second parameters can be changed easily without significant modification of the optical scheme, whereas it is necessary to rearrange almost all the optical elements for any spatial-frequency change. A spatial frequency of 1200 cycles/mm, which is close to the optimal value of the diffusion-recording mechanism in sillenite-family PRC,[3,12] was chosen for our version of the holographic interferometer. We measured dependency of the SNR on the input polarization and on the recording-beam intensity ratio in the course of this research to find the optimal configuration of the holographic interferometer.

When the object-beam noise (P_{NO}) was measured, the reference beam had always been shut down and the output analyzer A had been adjusted to close as completely as possible the object beam transmitted through the crystal. The rest of the object beam that was transmitted through crossed polarizers, with the crystal between them, is really the noise P_{NO} for the interferogram, because there is no information about the image reconstructed from the hologram in this light. The origin of such transmission stems from the nonideal quality of the dichroic sheet polarizers and from the localized stress-induced birefringence inside the PRC. In fact, the extinction rate [closed/open intensity ratio] of dichroic sheet polarizers, with BTO samples between them, is typically near 10^{-3}–10^{-4}. Note that a particular value of the extinction rate depends mainly on the sample region chosen for hologram recording and on the forces applied to the crystal by the sample holder (PRC's usually have high electro-optic and elasto-optic coefficients).

The reference-beam noise (P_{NR}) measurements are carried out each time the hologram has been recorded and completely erased in the crystal by a shutting down of the object beam. It was observed that when P_{NR} was measured just after some rearrangement of the recording beams, it was significantly smaller than when it was measured after a longer exposure. The angle ϑ between the recording beams was 43.5° for our particular setup; this corresponds to a spatial frequency of 1200 lines/mm. A small part of the reference beam can be scattered in the direction of the reconstructed image by nonuniformities of the real crystal in spite of the large angle between the beams. Usually such scattering takes place without change of the polarization state, and it seems that scattered light should be canceled by the use of the crossed analyzer in our scheme. But in reality this scattered light interferes with the reference beam and creates a noise hologram, and self-diffraction of the reference beam from such a noise hologram is accompanied by rotation of the polarization plane. So this scattered light successfully passes through the analyzer and produces an undesirable illumination in the reconstructed-image plane with an intensity comparable with that of P_{NO}.

When both recording beams are open, the hologram in the crystal begins to be recorded, the diffracted beam transmits through the crossed polarizers, and the diffraction-efficiency evolution is recorded by the digital oscilloscope. Both the stationary value of the diffracted-beam intensity $\mathbf{S}$ and the hologram recording time τ_R are of practical interest for the holographic interferometer and are calculated from oscilloscope tracks.

The hologram recording time τ_R was calculated from the temporal dependence of the diffraction efficiency for the initial period of the hologram recording. The diffraction efficiency of the volume hologram in a PRC can be evaluated from Eq. (3). Let us assume that the exponential increase of $\mathbf{E}_{SC}$ with time for the hologram recording process goes as follows:

$$\mathbf{E}_{SC}(t) = \mathbf{E}_{SC}{}^{ST}\left[1 - \exp\left(-\frac{t}{\tau_R}\right)\right], \tag{12}$$

where $\mathbf{E}_{SC}{}^{ST}$ is the saturated (maximal) value of the space-charge electric-field amplitude. If the suggestion of Eq. (12) is valid, the hologram diffraction efficiency must increase as

$$\eta(t) = \eta_{ST}\left[1 - \exp\left(-\frac{t}{\tau_R}\right)\right]^2. \tag{13}$$

Therefore the function

$$G_R(t) = \ln(1 - \sqrt{\eta(t)/\eta_{ST}}) \tag{14}$$

should be a straight line. But the experiment shows that it is impossible to obtain $G_R(t)$ in the form of straight line for any BTO sample and for any intensity (or polarization) of the recording beams when the hologram is recorded with a wavelength $\lambda = 0.6328$ μm. In order to compare the hologram recording time under different experimental conditions (different intensities of recording beams), we defined τ_R as the tilt of the asymptotic straight line with respect to the curve $G_R(t)$ at the initial moment of hologram recording.

5. EXPERIMENTAL RESULTS

Dependence of the Signal-to-Noise Ratio on Recording-Beams Polarization

Dependence of the steady-state diffraction efficiency (signal $\mathbf{S}_{ST}$) on the orientation of input polarizer (E, Fig. 1) is shown in Fig. 3 for the BTO53 sample. The zero position of the angle corresponds to the polarization's being parallel to the crystallographic axis [001] of the crystal (see Fig. 2). Note that this dependence was measured when the analyzer (A, Fig. 1) was oriented so as to close the transmitted object beam. This differs from well-known measurements[9] of a similar dependence that were carried out without an analyzer. In any case, our results are in good agreement with the data of Ref. 11. Indeed, the

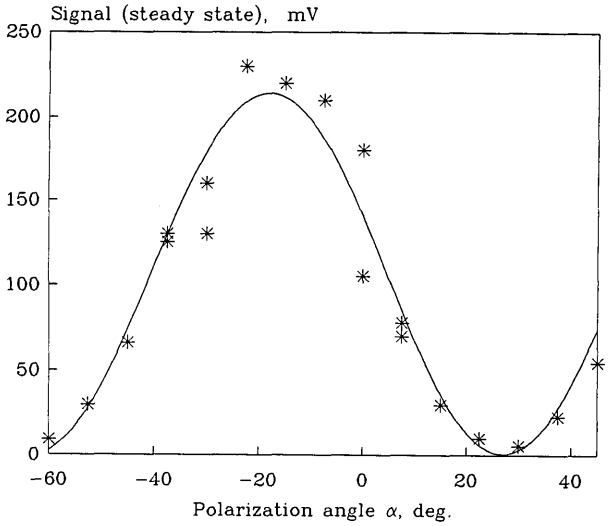

Fig. 3. Dependence of the signal value (output intensity) on the input light polarization for the BTO53 sample. α, angle between axis [001] of the crystal and the vector of the light polarization; asterisks, signal; solid curve, theory.

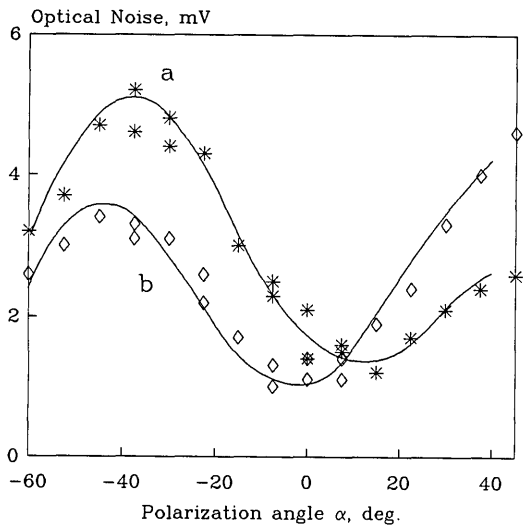

Fig. 4. Dependence of the power of the reference-beam noise P_{RE} (asterisks) and the object-beam noise P_{OB} (diamonds) on the input light polarization for the BTO53 sample. α, angle between axis [001] of the crystal and the vector of the light polarization; solid curves: a, P_{NR}; b, P_{NO}.

diffraction efficiency is independent of the reconstructing-beam polarization, but the angle γ between polarizations of transmitted and diffracted beams changes as follows[9,11]:

$$\gamma = \pi/2 - 2\alpha + \rho\mathbf{d}, \tag{15}$$

where α is the input polarization angle with respect to axis [001]. Therefore the intensity of the diffracted light that is transmitted through the closed analyzer should be

$$\mathbf{S}_{ST} = I_{RE}\eta \cos^2(2\alpha - \rho\mathbf{d}), \tag{16}$$

where η is the diffraction efficiency of the hologram. The theoretical curve associated with Eq. (16) is depicted as a solid curve in Fig. 3. Experimental data are in rather good accordance with the theory of anisotropic diffraction in a PRC of the sillenite family,[11] and the maximum of $\mathbf{S}_{ST}$ is observed when the recording-beam polarization is parallel to axis [001] in the middle plane of the sample. Here we have taken into account the natural optical activity $\rho\mathbf{d}$, which is 36° for BTO53.

Figure 4 presents measurements of both parts of the optical noise, for the BTO53 sample, with the same intensity of the recording beams used for the measurements depicted in Fig. 3 ($I_{OB} \simeq 0.35$ mW/cm^2, $I_{RE} \simeq 1.5$ mW/cm^2). The dependence of P_{NR} on the polarization angle is shown as curve a. One can see that this dependence has a maximum and a minimum that are shifted $\simeq 20°$ with respect to those of the signal dependence. This is an additional confirmation of the holographic nature of this part of the noise. Indeed, the input polarization angle $\alpha = \rho\mathbf{d}/2 + \pi/4$ ($\alpha = \rho\mathbf{d}/2 - \pi/4$) corresponds to a situation in which the polarization of the beam that is diffracted from a noisy hologram coincides with the scattered-beam polarization[8]—a fact that favors the holographic amplification (or attenuation) of a weak scattered beam. But in our setup configuration, the analyzer can transmit only that part of the light whose polarization is orthogonal to the reference beam: that is why the maximum (minimum) is observed for an input polarization angle that is shifted from the position $\alpha = \rho\mathbf{d}/2$ at approximately 20° (not at 45°). The polarization dependence of P_{NO} [curve b of Fig. 4] reflects an internal stress anisotropy and usually depends on the location on the sample at which the hologram has been recorded as well as on the construction of the sample holder.

The SNR versus the recording-beam polarization (Fig. 5) has an asymmetric form, owing to a shift between the signal curve and the noise curve. This dephasing is also the reason for the SNR's maximum shift from position $\alpha = \rho\mathbf{d}/2$. It should be emphasized that the two terms of the optical noise, P_{NR} and P_{NO}, depend on the polarization differently. Therefore the SNR's maximum position depends on the intensity of both the reference (I_{RE}) and the object (I_{OB}) beams if it is considered that in the first approximation P_{NR} is proportional to I_{RE} and P_{NO} to I_{OB}, with different proportionality coefficients n_R and n_O for each one. So, the optimal polarization of the recording beam depends on its intensity. Fortunately, the maximum of the curve SNR versus α is not very sharp, as

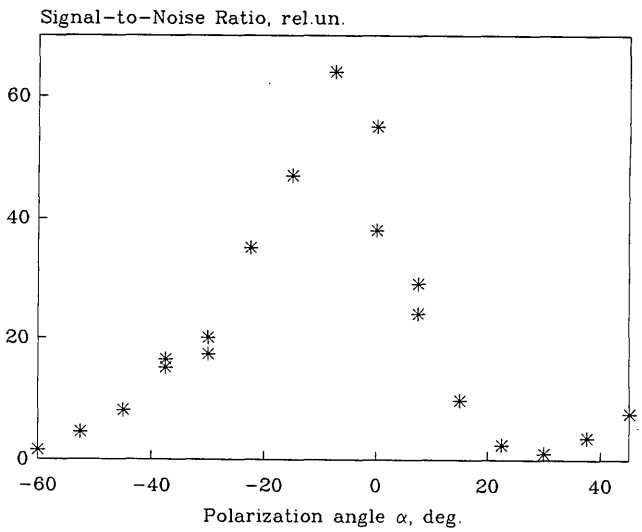

Fig. 5. Dependence of the SNR on the input light polarization for the BTO53 sample. α, angle between axis [001] of the crystal and the vector of the light polarization; rel. un., relative units.

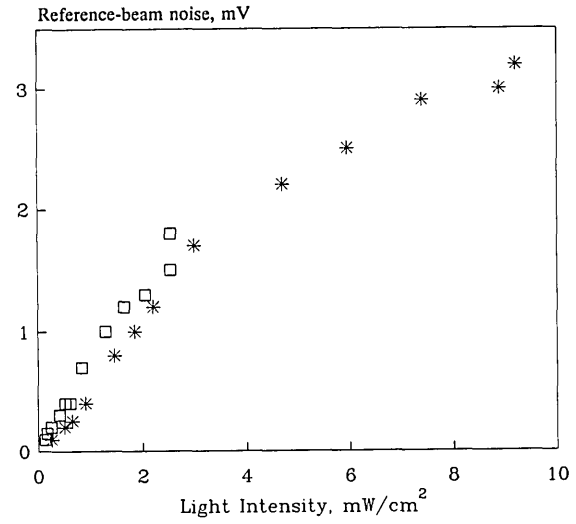

Fig. 6. Dependence of the power of the reference-beam noise component P_{NR} on the reference-beam intensity for BTO48 (asterisks) and BTO53 (squares) samples.

can be seen from Fig. 5. From a practical point of view this means that we are not obliged to do a high-precision adjustment of the input polarization of our holographic interferometer. But in some special cases the influence of the object-beam noise P_{NO} can significantly change the optimal position, and it is better to check experimentally each particular PRC sample.

Dependence of the Signal-to-Noise Ratio on Recording-Beam Intensity

Noise

It was observed that the object-beam noise P_{NO} is proportional with high precision to the object-beam intensity I_{OB}. This is not surprising, because this noise comes from a residual light transmitted through the crystal between two crossed polarizers. But the recording of the noise hologram makes the nature of reference-beam noise P_{NR} different and more complicated. The experimental dependence of P_{NR} on the reference-beam intensity is shown in Fig. 6 for both BTO48 and BTO53. One can see that these curves can be also approximated by a linear dependence for the intensity band that we used in our experiments.

Signal-to-Noise Ratio

Measurements of the signal and both optical noise components were independently carried out, as was described in Section 4. Hence we can calculate the SNR for the hologram reconstruction, by using either a reconstructed beam (the usual mode) or the self-diffraction effect. Here we present the experimental results supported by theoretical calculations for both cases. For the usual reconstruction mode the dependence of the SNR (when only P_{NR} is taken into account) on the reference-to-object-beam intensity ratio is shown in Fig. 7. The solid curve in this figure represents the theoretical dependence [Eq. (11) with $n_{OB} = 0$] fitted to experimental results. One can see from this figure that the maximum SNR is shifted from the position where $a = 1$ toward smaller values, as our theoretical consideration for holographic recording of complex waves in PRC's predicts.

One should take into account both noise components (P_{NR} and P_{NO}) in PRC's to optimize the dual-beam scheme of a holographic interferometer by using the self-diffraction effect. For this case the experimental dependence of the SNR on the recording-beam intensity ratio is shown in Fig. 8 for both BTO48 (asterisks) and BTO53 (circles) samples. These data were obtained when the reference-beam intensity I_{RE} was variable but the object-beam I_{OB} intensity was kept constant. The latter was chosen as high as possible. The obvious reason for this is the large losses of light produced by the scattering of the object surface. The solid curves are calculated from Eq. (11) with use of the sample parameters measured experimentally. The maximum SNR is achieved now when the reference intensity is five times higher than the object one. This is only because of the

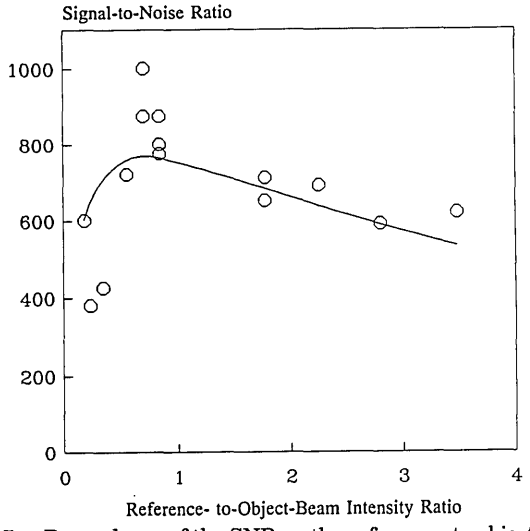

Fig. 7. Dependence of the SNR on the reference- to-object-beam intensity ratio for one-beam reconstruction of the hologram (only the noise component that is due to the reference beam is taken into account). Circles, experiment; solid curve, theory.

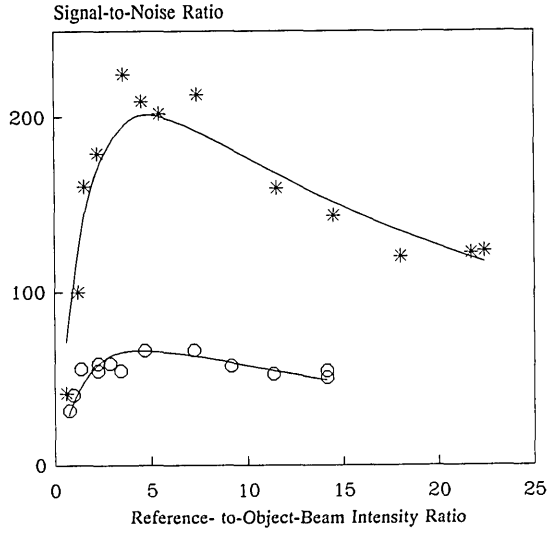

Fig. 8. Dependence of the SNR on the reference-to-object-beam intensity ratio for reconstruction of the hologram in a dual-beam interferometer (both object- and reference-beam noise are taken into account) for the BTO48 (asterisks) and the BTO53 samples (circles). Solid curves represent corresponding theoretical calculations.

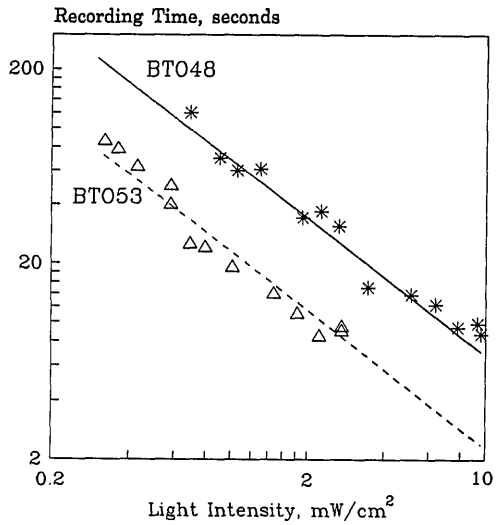

Fig. 9. Dependence of the hologram recording time τ_R on the recording-beam light intensity for the BTO48 (asterisks) and the BTO53 samples (triangles). Solid curve, theoretical calculation for BTO48; dashed curve, theoretical calculation for BTO53.

strong influence of the object-beam noise P_{NO} through the coefficient n_O in Eq. (11). The object-beam noise differs significantly from that in the case of the usual hologram reconstruction (see Fig. 7), whose optimal conditions correspond to a reference-beam intensity that is smaller than the object one.

One can see that the BTO48 sample shows a higher SNR than does the BTO53 sample. The main reason for this difference is diffraction efficiency, since the noise parameters were found to be very similar for both samples. But a difference in crystal thicknesses ($\mathbf{d}$ = 8.0 mm for BTO48 and $\mathbf{d}$ = 6.1 mm for BTO53) is not enough to explain a nearly 10-times difference in diffraction efficiency. The explanation of the difference is not clear at present and is beyond the scope of this study.

Hologram Recording Time

The intensity dependence of the hologram recording time τ_R, as defined in Section 4, is presented in Fig. 9 for both BTO48 and BTO53. The dependences are plotted on a log–log scale for easy estimation of crystal sensitivity. The abscissa axis in Fig. 9 corresponds to the sum of the recording-beam intensities $I_{RE} + I_{OB}$. It is quite clear that our experimental data are well fitted by the calculated curves shown as a solid line for BTO48 and as a dashed line for BTO53 samples. We assumed that τ_R varies in inverse proportionality to the recording-beam intensity:

$$\tau_R(I_{RE} + I_{OB}) = C_R . \tag{17}$$

In Eq. (17) C_R is a constant calculated from experimental data. One can see that the BTO53 sample has a sensitivity three times higher than that of BTO48. This fact also shows a difference between the measured crystals, but there is no explanation for this difference yet. We can only note that the two single crystals were grown in similar experimental conditions but with compounds supplied by different firms.

6. DISCUSSION

The experimental data of Figs. 5–9, supported by theoretical considerations, allow us to find the optimal configuration of optical elements for a photorefractive holographic interferometer. However, we must note that we are always limited by the available laser power, P_L, which defines the intensity of the recording beams. The sum of the recording-beam intensities, $I_{OB} + I_{RE}$, defines the hologram recording time τ_R, as can be seen from Fig. 9.

With respect to the choice of τ_R, we recommend that it be set as small as possible, because a longer time means slower transmission of interferometry information and a failure in the stability of the holographic interferometer. Following Ref. 13 and assuming that the object is illuminated by light with power $P_L\beta$, we can obtain the intensity of the object beam in the crystal plane:

$$I_O = \frac{P_L R\beta}{S_O} \frac{1}{16\mathcal{F}^2(1+q)^2}, \tag{18}$$

where R is the coefficient of reflectivity of the object surface (per steradian in the direction of the projection lens), β is the beam-splitter coefficient, S_O is the surface area of the object, $\mathcal{F}$ is the f-number of the projection lens ($\mathcal{F} = F/D$, where D is lens diameter and F is the focal length), and q is the lateral magnification coefficient of the projection system. If the remaining part of the laser light is used as a reference beam with total power $P_L(1-\beta)$, then the intensity of this beam in the crystal plane is

$$I_R = \frac{P_L(1-\beta)}{q^2 S_O} . \tag{19}$$

For large objects the magnification coefficient, $q \ll 1$, and the final expressions for the recording time and the reference-to-object-beam intensity ratio usually may be rewritten as

$$\tau_R \approx \frac{S_O}{P_L} \frac{16\mathcal{F}^2 q^2 C_R}{16\mathcal{F}^2(1-\beta) + q^2 R\beta}, \tag{20}$$

$$a \approx \frac{16\mathcal{F}^2}{Rq^2} \frac{(1-\beta)}{\beta} . \tag{21}$$

Using expressions (11), (20), and (21) and substituting the parameters of the real setup, one can choose a compromise between the SNR and the response time of the interferometer.

It is easy to see from relation (20) that the larger the object area that we want to study, the longer the hologram recording time we will need. Thus a more sensitive crystal allows one to study larger object areas with the same laser power. The same conclusion was made by Troth and Dainty.[12] In their work one can find estimations of the maximum object area that can be studied with a photorefractive holographic interferometer that contains BTO crystals. The working wavelength that they used was 0.5145 μm.

We studied two BTO samples with different holographic parameters and found that BTO53 is preferable for obtaining high-quality holographic interferograms because of its higher sensitivity. The main reason for this result

is the lower influence of the mechanical and thermic instabilities of the interferometer when the hologram recording time is small. But for some special applications a sample with a higher SNR could be better, for example, if we wish to obtain time-average interferograms of a vibrating object that has a high vibration amplitude. With our particular interferometer, after its optimization we obtained good-quality interferograms (with SNR = 50) of an object of $\approx$50 cm^2 area, using a BTO48 sample with $\tau_R = 25$ s.

7. CONCLUSIONS

We have shown that the holographic formation in PRC's of images with complex wave fronts is different from that in the case of a plane wave front and should be taken into account for optimization of the holographic setup or when estimation of the holographic parameters is needed (information capacity, for example). The theoretical analysis presented here does not take into account all the peculiarities of photorefractive crystals. In particular, the effects of reconstructed-beam wave-front disturbances that are due to the nonlinearity of the holographic recording, the dynamic hologram-enhancement effect, and the volume character of the hologram were not estimated in our calculations. Nevertheless, any of them could change the expressions that we obtained for the reconstructed-beam amplitude [Eq. (5)] and intensity [Eq. (6)]. In any case, a good fit with experimental data shows that this approach can be used as a first approximation for calculating and designing the optimal optical schemes of holographic systems that use PRC's and operate with complex images.

In this paper we also present an experimental approach to finding the optimal configuration of optical elements in a holographic interferometer with PRC's, by considering signal-to-noise ratio as one of the important parameters. It is shown that both terms of the optical noise (resulting from the object and reference beams) influence the optimal position and that the sensitivity of the crystal, which defines the hologram recording time, can limit the size of the object to be studied.

ACKNOWLEDGMENTS

This research was partly supported by the Conselho Nacional de Desenvolvimento Científico e Technológico do Brasil (CNPq). We thank Diana Tentori and M. P. Petrov for fruitful discussions and Victor V. Prokofiev from the A. F. Ioffe Institute in St. Petersburg, Russia, for the high-quality BTO crystals used in this research. During his stay at the Centro de Investigación Científica y de Educación Superior de Ensenada, S. Miridonov was supported by the Dirección Adjunta de Investigación Científica, Consejo Nacional de Ciencia y Technología.

REFERENCES

1. J. P. Huignard and J. P. Herriau, "Real-time double-exposure interferometry with $Bi_{12}SiO_{20}$ crystals in transverse electrooptic configuration," Appl. Opt. **16,** 1807–1809 (1977).
2. J. P. Huignard and A. Marrakchi, "Coherent signal beam amplification in two-wave mixing experiments with photorefractive $Bi_{12}SiO_{20}$ crystals," Opt. Commun. **38,** 249–254 (1981).
3. A. A. Kamshilin and M. P. Petrov, "Continuous reconstruction of holographic interferograms through anisotropic diffraction in photorefractive crystals," Opt. Commun. **53,** 23–26 (1985).
4. A. A. Kamshilin and E. V. Mokrushina, "Comparison of dual-beam schemes for simultaneous writing and reading of volume holograms in photorefractive crystals of the type $Bi_{12}SiO_{20}$," Sov. Tech. Phys. Lett. **16,** 330–331 (1990).
5. J. Joseph, K. Singh, and P. K. C. Pillai, "Crystal orientation dependence of the SNR for signal beam amplification in photorefractive $BaTiO_3$," Opt. Laser Technol. **23,** 237–240 (1991).
6. R. C. Troth, S. L. Sochava, and S. I. Stepanov, "Noise and sensitivity characteristics of $Bi_{12}SiO_{20}$ for optimization of a real-time self-diffraction holographic interferometer," Appl. Opt. **30,** 3756–3761 (1991).
7. G. S. Trofimov and S. I. Stepanov, "Photorefractive $Bi_{12}SiO_{20}$ crystal for holographic interferometry at $\lambda = 0.63$ μm," Sov. Tech. Phys. Lett. **11,** 256–257 (1985).
8. A. Marrakchi, J. P. Huignard, and P. Gunter, "Diffraction efficiency and energy transfer in two-wave mixing experiments with $Bi_{12}SiO_{20}$ crystals," Appl. Phys. **24,** 131–138 (1981).
9. M. P. Petrov, S. V. Miridonov, S. I. Stepanov, and V. V. Kulikov, "Light diffraction and nonlinear image processing in electrooptic $Bi_{12}SiO_{20}$ crystals," Opt. Commun. **31,** 301–305 (1979).
10. J. W. Goodman, *Statistical Optics* (Wiley, New York, 1985).
11. A. Marrakchi, R. V. Johnson, and A. R. Tanguay, Jr., "Polarization properties of photorefractive diffraction in electrooptic and optically active sillenite crystals (Bragg regime)," J. Opt. Soc. Am. B **3,** 321–336 (1986).
12. R. C. Troth and J. C. Dainty, "Holographic interferometry using anisotropic self-diffraction in $Bi_{12}SiO_{20}$," Opt. Lett. **16,** 53–55 (1991).
13. R. W. Boyd, *Radiometry and the Detection of Optical Radiation* (Wiley, New York, 1983).